Journal of ELECTRICAL ENGINEERING, VOL 71(2020), NO5, 308–316

sciendo

PAPERS

A novel planar, broadband, high gain lateral wave antenna array for body scanning applications

Fikret Tokan[1], Daniele Cavallo[2], Andrea Neto[2]

Three-dimensional body scanning systems are increasingly used in sensitive public areas such as airports. By providing a high resolution image of a person from all sides, it is possible to detect potential metallic, ceramic and explosive threats. For these systems, it is essential to design broadband antennas with a fan beam, highly directional radiation in one plane and wide in the other plane, and characterized by phase center stability as a function of frequency. In this paper, the planar lateral wave antenna (LWA) array is proposed to achieve these radiation requirements. The LWA has two critical shortcomings: the flaring part and the dielectric matching layers (MLs), to operate over very broad frequency bands. In this work, these shortcomings are overcomed by forming a connected array of planar LWAs to improve broadband performance and by applying necessary perforations on the dense dielectric lens antenna to create different effective relative permittivity regions. An eight element connected and perforated LWA array is designed to operate in the 8–24 GHz frequency band. The drilled holes are proved to play a similar critical role of MLs in internal reflection suppression. The results emphasize all crucial demands for body scanning systems.

K e y w o r d s: connected array, dielectric lens antenna, dielectric matching layers, perforated lens

1 Introduction

In the field of security screening, new imaging technologies are being developed for the detection of concealed weapons or explosives, in order to protect the civilians in sensitive public areas such as airports. Millimeter wave (mm-wave) three-dimensional body scanning systems are the most promising ones since modern threats including plastic or ceramic handguns and knives, as well as extremely dangerous plastic and liquid explosives, can be detected with high resolution images. Besides, it is not harmful for human since mm-wave radiation is a non-ionizing solution that is considered safe [1]. Three-dimensional body scanning systems are typically realized with linear arrays composed of separate antenna elements capable of providing a highly focused beam in one plane and a broad fan beam in the other plane [2]. This is because the lateral resolution is defined in one plane by the narrow beamwidth of the antenna array and in the other plane by a mechanical sweep and synthetic aperture imaging techniques. Flat lens concepts have been proposed to achieve fan-beam radiation patterns in [3, 4], but most designs operate over limited frequency ranges. A concept to achieve a flat lens with wide bandwidth was proposed by these authors in [5] and was referred to as the lateral wave antenna (LWA). The LWA provides, over a broad frequency bandwidth, highly directive radiation in one plane, broad beam in the other plane and phase center stability as a function of the frequency. Indeed, when phase centers of radiation for each of the orthogonal planes move as a function of the frequency, time consuming compensation algorithms should be employed [5]. In this work, the scope is to introduce an array of LWAs, with the aim to reduce the complexity of the antenna in terms of assembly and manufacturability. The structure of LWA, shown in Fig. 1, consists of a dielectric filled parallel plate waveguide (PPW) that supports the propagation of a TEM wave. To convert the cylindrical wavefront propagating in the PPW into a planar wavefront, the structure is truncated to become a planar lens. High dielectric material $\varepsilon_r = 9.8$ is chosen as dielectric material to couple most of the power from the feed points into the dielectric. However, when the relative permittivity of the selected lens material is high, considerable amount of internal reflections occur at the high dielectric-air interface [6, 7]. The internal reflections deteriorate the return loss and the radiation characteristics of the antenna. Thus, in order to reduce the internal reflections and consequently achieve a broadband impedance matching, three matching layers are added at the open end of the lens structure. Moreover, in order to facilitate the smooth transition to free space, a short metallic flaring is also added after the matching layers. The measurement results of LWA highlighted highly directive fan beam radiation and frequency stable phase centers, over a bandwidth exceeding 3:1 [5]. Lateral wave excitation and the radiation mechanism (Cherenkov radiation) of the antenna are investigated in [5] and are not repeated here, for the sake of brevity.

Although the LWA satisfies the above mentioned necessary requirements for three-dimensional body scanning

[1] Department of Electronics and Communications Engineering, Faculty of Electrical and Electronics, Yildiz Technical University, Istanbul, ftokan@yildiz.edu.tr, [2] Microelectronics Department, Faculty of Electrical Engineering, Delft University of Technology, Delft, Netherlands

DOI:10.2478/jee-2020–0042, Print (till 2015) ISSN 1335-3632, On-line ISSN 1339-309X

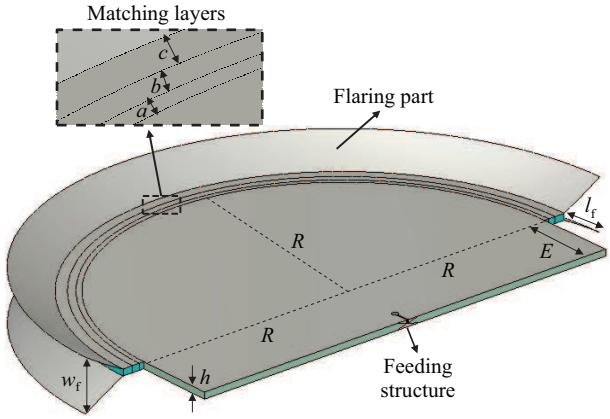

Fig. 1. Quasi-planar lateral wave antenna

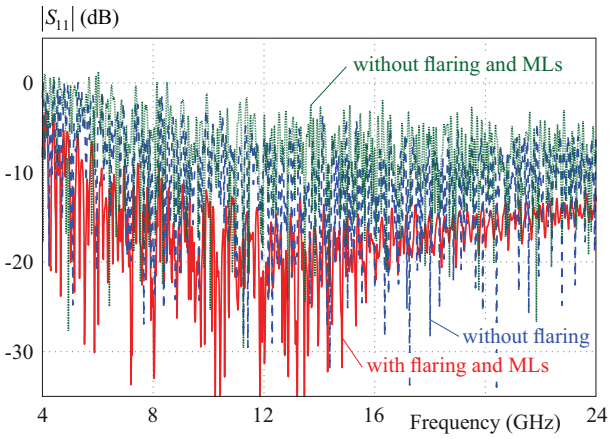

Fig. 2. The reflection coeffients of LWA with three different design scenarios: With both flaring and MLs, without flaring and without flaring and MLs

antenna system, it has two critical shortcomings that increase the complexity of the assembly during manufacturing: (1) the flaring part and (2) matching layers. The metallic flaring is added to allow radiation, so that the open end of the PPW is at least half a free space wavelength at the lowest operational frequency. Therefore, the antenna structure is quasi-planar and it cannot be manufactured resorting to standard printed circuit board technology. Adding matching layers is also required to implement a smooth transition to air and consequently achieve broadband impedance matching. Possible parasitic effect due to air gaps between these layers can become problematic especially for high frequency applications [8]. Besides, adding three different MLs increases the manufacturing cost of the antenna due to bonding processes. The necessity of both flaring part and MLs for broadband impedance matching is highlighted in Fig. 2. It is clear from Fig. 2 that the reflection coefficient of the LWA without flaring and MLs has the highest value, which is above -5 dB in the whole frequency band. When MLs are added at the radiating end of the antenna, but still without flaring, the reflection coefficient is slightly decreased. However, this level is still higher than -10 dB within the broad frequency band. When including also the metal flaring structure, the LWA achieves a reflection coefficient lower than −10 dB in the 8–24 GHz frequency band.

In this work, a novel, planar, broadband, high gain lateral wave antenna array is proposed and designed in 8–24 GHz frequency band. The array elements do not necessitate flaring parts and MLs with different dielectrics. Thus, a fully planar printed circuit board implementation is obtained. This is achieved by composing a connected planar LWA array. It is shown that mutual coupling between array elements is essential and has a beneficial effect for broadband operation. Furthermore, a perforated structure is obtained by drilling holes in the dielectric slab to approximate lower effective dielectric constants and realize a smooth transition between dielectric and air. By drilling holes in the lens core of the LWA, only one dielectric material is used in the design rather than using one material as lens core and three different materials as MLs. The separation between the holes is kept small compared to the operating wavelength; under this assumption, the perforated dielectric substrate can be approximated as an equivalent uniform dielectric with a desired relative permittivity. These design improvements decrease the cost and complexity of the manufacturing process and makes the connected planar perforated antenna array a perfect candidate for 3-D body scanning systems. The analysis of the dielectric lens antennas is carried out using three dimensional full-wave electromagnetic (3-D EM) simulator of CST Microwave Studio time-domain solver [9].

The proposed antenna can be compared to horn antennas which can also be used for the considered application. However, while H-sectoral horns also provide a fan beam radiation, they are characterized by smaller frequency bandwidth compared to the presented solution [10, 11]. This is mainly due to the waveguide feed that limits the relative bandwidth. Although Transverse Electromagnetic (TEM) horn has been demonstrated to achieve excellent bandwidth [12, 13], this solution is known to be affected by a shift of the phase center as a function of frequency. One of the advantage of the proposed solution with respect to TEM horn is the non-dispersive behavior,

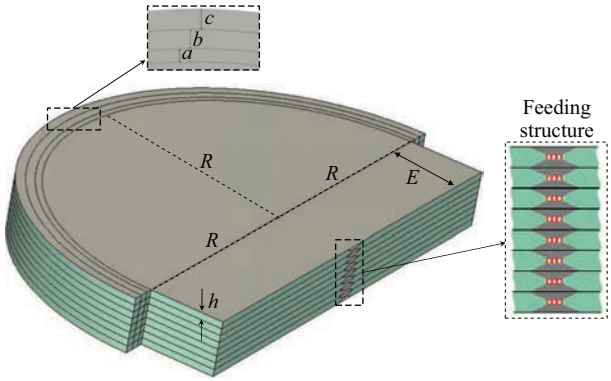

Fig. 3. Connected LWA array with its feeding structure, each element has three MLs

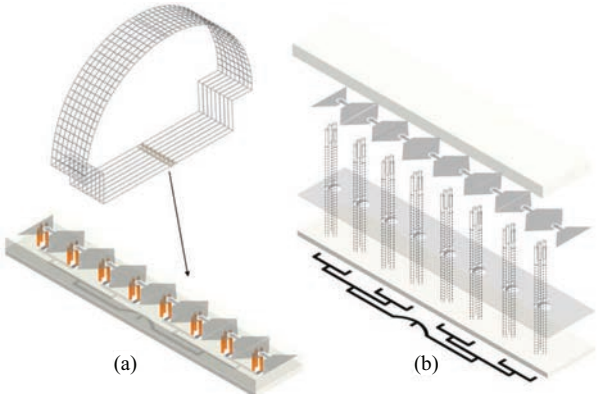

Fig. 4. Possible implementation of the feeding network: (a) – three-dimensional perspective view; (b) – exploded view of the multi-layer stack up

since the phase center location of the lateral wave radiation mechanism is independent from the frequency [14].

2 Connected LWA array

In standard narrowband array designs, the objective is to keep low mutual coupling between the radiating elements not to alter too much the performance of each isolated element. In recent years, a new approach has arisen for the design of broadband arrays, in which high mutual coupling between the array elements is intentionally introduced to enhance the bandwidth [15–18]. A simple way to enhance the coupling between neighboring elements is to bring them closer to each other. A connected array can be briefly described as an array of antennas which are electrically connected to each other. Therefore, in this work we stack several lateral wave antennas together in a connected array environment, with the aim of achieving broadband impedance matching thanks to the enhanced mutual coupling.

2.1 Array design

A connected array composed of LWAs is designed, as shown in Fig. 3, with its feeding structure. Each LWA consists of a parallel plate waveguide structure made of copper, $\sigma = 5.8 \times 10^7$ filled by Rogers TMM10i with relative permittivity $\varepsilon_r = 9.8$ and dielectric loss tangent value of 0.0022. Physical dimensions of each element are adjusted for the target operation bandwidth of 8 to 24 GHz. The thickness of each array element, $h = 2.54$ mm and total thickness of the array $(8 \times h)$ is 20.32 mm. This total aperture size is almost equal to the width of the flaring (W_f), shown in the original single antenna design in Fig. 1. Thus, the total height if the array is at least half of the free space wavelength at the lowest operational frequency. The shape of each PPW consists of a semi-circular part, with radius R which is 40.25 mm, and a rectangular extension base, characterized by $E = 0.35R$, to approximate an elliptical profile. Three matching layers are utilized to support free space radiation formed from dielectric materials RogersTMM6 ($\varepsilon_r = 6.3$, loss tangent$= 0.002$), RogersTMM4 ($\varepsilon_r = 4.7$, loss tangent$= 0.0027$) and Rexolite ($\varepsilon_r = 2.54$, loss tangent$= 0.0009$) and thicknesses $a = 1.77$ mm, $b = 2.65$ mm, $c = 3.79$ mm, respectively.

The feeding structure of the array is composed of 8 lumped ports, one for each slot, that are connected to a bow-tie tapered transition to improve matching performance, as shown in the inset of Fig. 3. This feeding

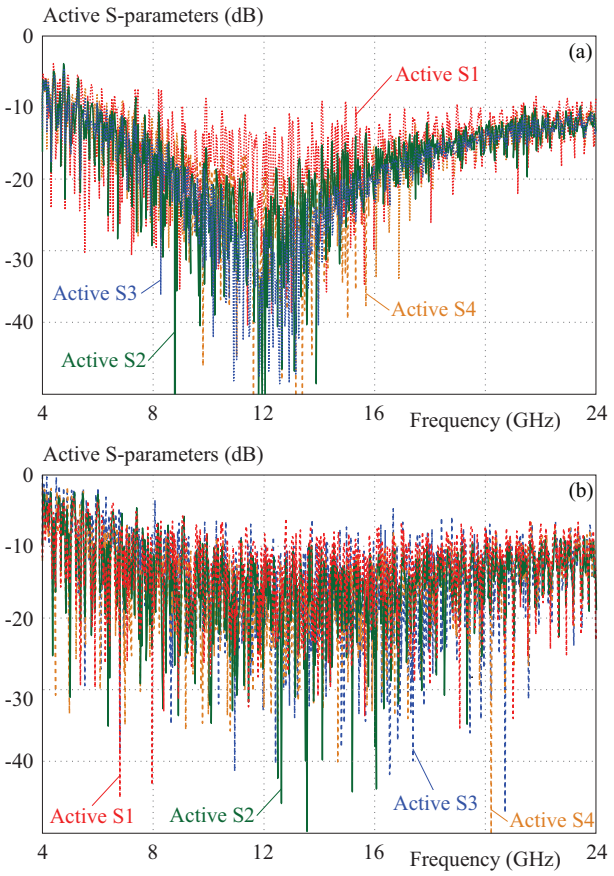

Fig. 5. Active S-parameters of the connected array elements (a) – with MLs, (b) – without MLs

supports the lateral wave propagation on the interface between free space and the dielectric. A possible implementation of the feed is depicted in Fig. 4. It consists of 8 tapered feeds with a co-planar waveguide excitation, connected through vias to a lower metal layer, where a microstrip corporate feed network is used to provide a 1-to-8 power combiner.

2.2 Active S-parameter calculations

While the conventional impedance matching parameter for an antenna element is S_{11}, in an array environment, the active reflection coefficient should be investigated. It can be described as the percentage of power reflected back from the radiating element when all array elements are simultaneously excited. Considering equi-phase and equi-amplitude excitation of the array for broadside radiation, the active reflection coefficient Γ_m can be calculated as follows [18]:

$$\Gamma_m(\theta) = \sum_{n=1}^{N} S_{mn} e^{-jknd\sin\theta}, \qquad (1)$$

where $k = (2\pi/\lambda)$, m is the index indicating the mth array element and S_{mn} is the transmission coefficient from port n to port m. d is the spacing between the array elements and θ is the beam steering angle. In our application all array elements radiate to broadside direction, thus θ is taken as zero in active reflection coefficient calculations. In this equation, the mutual coupling between array elements is taken into account, thus an array element can achieve broadband active impedance matching even if it has poor isolated S_{11}. Indeed, the LWA without flaring part has very poor reflection coefficient value as demonstrated in Fig. 2. However, as shown in Fig. 5(a) in a connected array environment, active reflection coefficients of each array element are lower than -10 dB in the operation frequency band, thanks to the favorable coupling effect between elements. The elements of the connected array are enumerated from bottom to the top of the structure.

Thus, the variation of Γ_1 with frequency is obtained for the bottom element of Fig. 3. Due to the symmetrical placement of each element with respect to the center of the array, the curves Γ_1, Γ_2, Γ_3 and Γ_4 are equal to Γ_8, Γ_7, Γ_6 and Γ_6, respectively. When an array is large enough, the central element performs similar to an element embedded in an infinite array, whereas the edge elements of a finite array behave differently from the inner ones. These finite edge effects are clear from Fig. 5(a), where the active reflection coefficient of the edge element Γ_1 has the highest value. However, all the active reflection coefficient remain lower than -10 dB, within the frequency band under consideration.

Figure 5(a) demonstrates that each of the planar elements can achieve broadband impedance matching in the connected array environment without need for the flaring parts. The active reflection coefficients of the array elements when the MLs are not employed at the open end of the lens structure are reported in Fig. 5(b). It can be observed that the active reflection coefficients of the array elements are excessively high due to the dielectric contrast at the high dielectric-air interface. Figure 5(b) proves the necessity of MLs for smooth transition of radiation to free space in high dielectric applications.

2.3 Influence of matching layers on power flow inside the connected array

In dense dielectric lens antennas, deterioration in radiation characteristics occurs due to the strong internal reflections inside the lens. The intensity of these internal reflections is directly proportional to the dielectric contrast between lens and air. The influence of strong internal reflections on the active reflection coefficient of each array element is illustrated in Fig. 5. The power reflected from the dielectric-air interface corrupts the radiation characteristics as well as the return loss. The Poynting vector inside the connected LWA array with and without MLs is shown in Fig. 6. The reflected power is simulated using CST software. The power flow given in Fig. 6(a) demonstrates the presence of Cherenkov radiation in to the dense dielectric. Thanks to the properly applied dielectric MLs to the top of the connected LWA elements, a smooth transition is achieved from dielectric to free space. The power inside the connected LWA elements cannot be

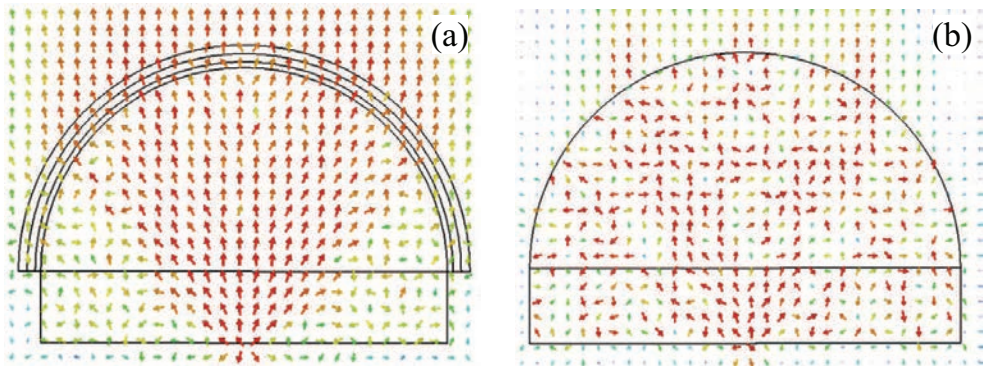

Fig. 6. Power flow for connected LWA elements: (a) – with three MLs, (b) – without MLs

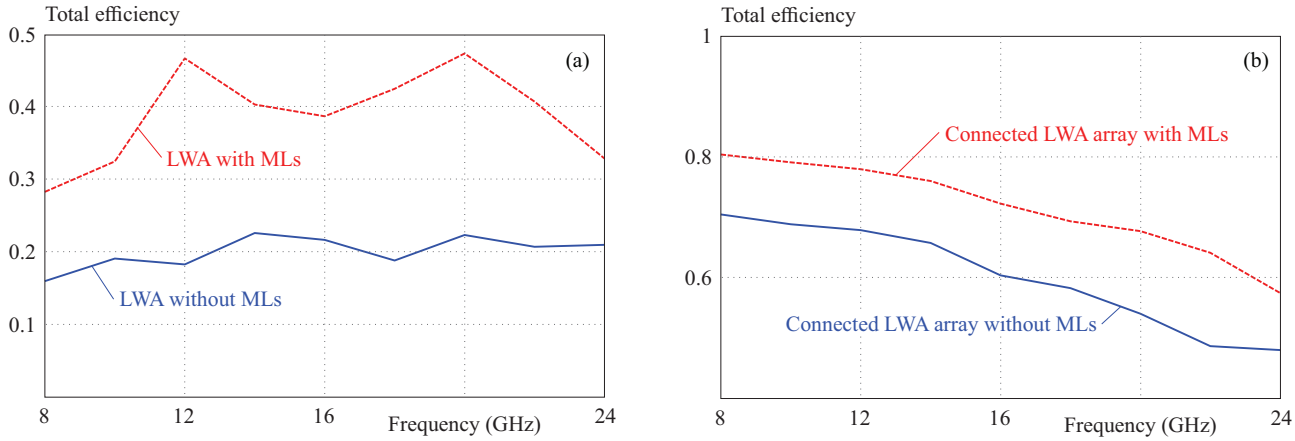

Fig. 7. The influence of dielectric MLs on the total efficiency of: (a) – planar LWA; (b) – connected LWA array

directed to the broadside direction properly in the without MLs design, as highlighted in Fig. 6(b). When power flows in Fig. 6(a) and (b) are compared, it can be easily observed that not only the strength but also the amount of the internal power reflections are considerably higher in the array design without MLs. The power reflected from the dense dielectric-air interface will contribute to radiation to arbitrary directions rather than to broadside direction, therefore side lobe levels of the radiation pattern will dramatically increase when MLs are not employed to the top of the connected LWA array elements. In Fig. 7, total efficiency variations of the planar LWA and the connected LWA array with and without MLs are given. The efficiency includes ohmic and mismatch losses. The total efficiency of planar LWA without MLs is around 0.2 at the whole operation frequency band where the total efficiency is between 0.3 and 0.5 in the same frequency band when three MLs are employed as given in Fig. 7(a). Higher total efficiency value is obtained when MLs are utilized since impedance mismatch loss of planar LWA is considerably higher without dielectric MLs as given in Fig. 2.

The total efficiency of connected LWA array without MLs has the highest value of 0.7 at the lowest frequency of the operating frequency band and this value decreases to 0.48 at the highest frequency of the band due to increase of dielectric loss with the frequency. Besides, the total efficiency of the connected LWA array with MLs is almost 0.1 higher since the return loss of array elements with MLs are considerably lower than the array elements without MLs as given in Fig. 5(a). Due to the increase in dielectric losses of an antenna at high frequencies, the total efficiency of connected LWA array highlighted in Fig. 7(b) decreases to 0.6 at 24 GHz.

3 Perforated LWA array design

When dealing with dense dielectric materials, internal resonances are excited within the lens, resulting in gain reduction, beam distortions and increase of side lobes as well as significant deterioration of the input impedance of each radiating element [19]. The most common way to considerably minimize these undesirable effects for narrowband applications is coating the top of the antenna with quarter-wave dielectric layer [8]. In wideband applications, a multi-layer coating having optimized thicknesses should be applied [20]. This approach requires the fabrication of different dielectric materials and the assembly of the multi-layer structure to top of the lens surface. In elliptical lens types such as the LWA, small air gaps may remain between the lens and the coating due to the

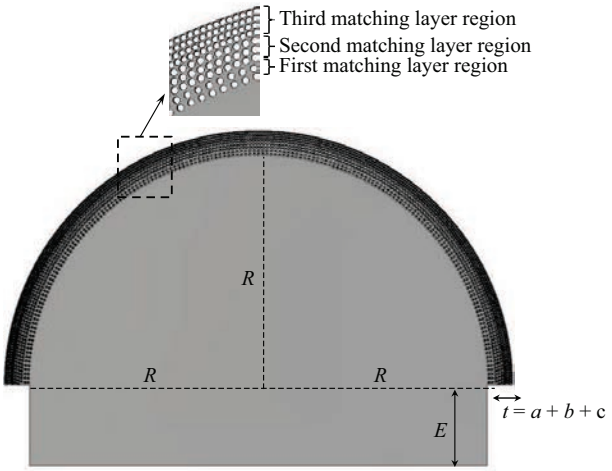

Fig. 8. Perforated LWA structure designed for 8–24 GHz

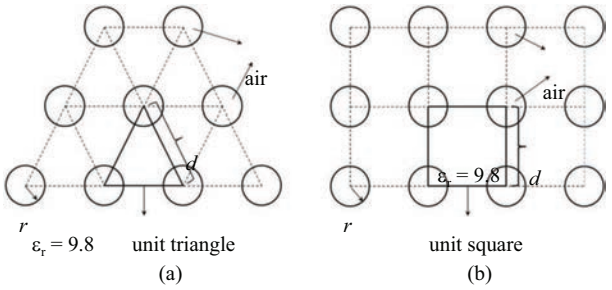

Fig. 9. Perforated dielectric material structure with: (a) - triangular, (b) – square lattices

inaccuracy of the surface curvatures. Placing linear or circular corrugations on the open end of lens surface can be a reasonable solution to significantly reduce these undesirable internal reflection effects [21]. Strong internal reflections can also be minimized using wave transformers made of homogeneous [19] or artificial [22] dielectrics at the top of the lens antenna. In this work, a perforated structure is designed by drilling periodic holes in the dielectric slab to create regions of equivalently lower dielectric constants. In this way, only one dielectric material is used in the design rather than using one material as lens core ($\varepsilon_r = 9.8$) and three other different materials ($\varepsilon_r = 6.3$, $\varepsilon_r = 4.7$ and $\varepsilon_r = 2.54$) as MLs. These design improvements can decrease the cost as well as the complexity of the manufacturing process.

3.1 Perforated dielectric design

The high dielectric lens core of LWA is extended as much as the width of MLs given in Fig. 3, for the perforated design. The radius of the semi-circular lens R, width of dielectric extension E and thickness of dielectric lens h given in Fig. 5 are set as 40.62 mm, $0.35 \times R$ and 2.54 mm respectively. The widths of MLs are also recalculated to for the target bandwidth as $a = 1.77$ mm,

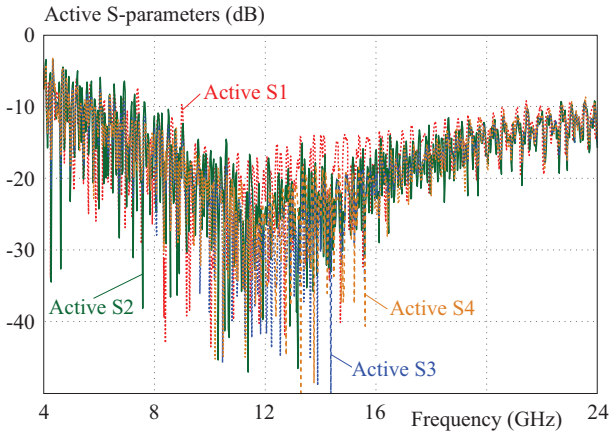

Fig. 10. The active S-parameters of perforated LWA array elements

$b = 2.65$ mm, $c = 3.79$ mm. Hence, the total radius of semi-circular part of the lens is equal to $R + a + b + c = 48.83$ mm. The perforated LWA is obtained by drilling holes in the extended part of lens surface as given in Fig. 8.

The effective relative permittivity of a dielectric material can be altered by perforating the substrate. The perforation is implemented as uniform square lattices for the first and second ML regions and as a triangular lattice of holes drilled through the high dielectric substrate for the third ML region. In this way, a higher air filled volume and consequently a lower effective relative permittivity is achieved in the third ML region by applying a triangular lattice, since the holes can be packed closer than for the corresponding square lattice [23]. A perforated dielectric substrate with either a rectangular or triangular lattice is depicted in Fig. 9. The dielectric perforation is performed with air holes, and for simplicity, each hole of the ML regions has a uniform diameter through the layers. To approximate the perforated dielectric as homogenous at the desired operating frequency band, the lattice spacings d and hole radius of each layer region r_1, r_2, r_3 are limited to half of the guided wavelength at the highest frequency [24]. The density of perforations in the substrate controls the effective relative permittivity of each region. In order to derive equations based on these models, a unit cell concept is adopted for both triangular and square lattices as given in Fig. 9. The effective relative permittivity ε_{eff} of each region can be calculated by the following equation if we consider the orientation of electricfield perpendicular to the axis of perforations [25]

$$\varepsilon_{\text{eff}} = \varepsilon_m + 2f\varepsilon_m \frac{\varepsilon_i - \varepsilon_m}{\varepsilon_i + \varepsilon_m - f(\varepsilon_i - \varepsilon_m)}, \qquad (2)$$

where ε_m and ε_i are relative permittivies of lens material and air, respectively and f denotes crucial parameter of the porous materials called porosity or simply a volume fraction. The porosity lies between 0 and 1 and is often given in percent. It can be defined as $\pi(r^2/d^2)$ and

Table 1. Perforation characteristics applied to the LWA

ML region	Lattice type	ε_{eff}	f_1	Hole radius (mm)	Number of holes
1-st	square	6.3	0.58	0.45	342
2-nd	square	4.7	0.71	0.5	649
3-rd	triangle	2.84	0.78	0.4	1232

$\pi r^2/d^2 \sin(\pi/3)$ for our square and triangular lattices, respectively. Considering polarization of electric field parallel to the axis of perforations, the effective relative permittivity is determined as

$$\varepsilon_{\text{eff}} = f\varepsilon_i + (1-f)\varepsilon_m \,. \tag{3}$$

Each of the planar LWAs in Fig. 3 needs three dielectric matching layers to support a smooth transition to free space in broad frequency band. The relative dielectric constants of the utilized dielectric materials are 6.3, 4.7, 2.54, thus it is aimed to obtain these effective permittivity values in each matching layer region by appropriate hole spacing. In the first ML region, 342 holes having 0.45 mm radius are considered to approximate the relative permittivity of region to 6.3 which corresponds to 0.58 volume fraction of air; 649 holes with 0.514 mm radius are obtained in the second ML region. Here, greater air-dielectric volume ratio of 0.71 is used to approximate 4.7 relative permittivity value. In the outermost ML region, a triangular lattice is selected since lower effective relative permittivity values can be achieved. Namely, when a triangular lattice of perforations is applied to a dense dielectric material, with $\varepsilon_{r_2} = 9.8$ and $r/d = 0.475$, $\varepsilon_{\text{eff}} = 2.84$ can be obtained, while for the same r/d value and a square lattice, an effective relative permittivity value of 3.2 occurs. Thus, 1232 holes are drilled in the outermost layer region of the lens. The radius of the holes is 0.4 mm and the effective relative permittivity of the region is approximately 2.84. It should be noted that by drilling extra narrower cylindrical holes between the larger holes in the material, it is possible to create a lower ε_{eff} value. However, drilling narrower holes next to wider holes will remove the simplicity of perforation process. The number of holes, their radius in each ML region and the synthesized effective relative permittivity values of the regions are given in Tab. 1. The radius of the circular holes is determined considering the machining accuracy (generally 0.1 mm). It is clear from Tab. 1 that the volume ratio of air is 0.78 which yields an effective permittivity of 2.84.

Although this value is higher than the target value of 2.54 for the outermost region, the active S-parameters of perforated LWA array elements given in Fig. 10 proves that the perforations on the dense dielectric lens material play a similar crucial role of the homogeneous dielectric MLs. The active S-parameters of the perforated LWA array elements are shown in Fig. 10 to achieve broadband impedance matching. Note that since VSWR describes the power reflected from the antenna which is the function of the reflection coefficient, the active VSWR level of each antenna element of the perforated LWA array will be lower than 2 in the whole operation frequency band.

4 Radiation characteristics of connected and perforated LWA array

In this section, the radiation characteristics of connected and perforated LWA array are investigated by comparing radiation patterns and directivity versus frequency. The simulated radiation patterns of connected and perforated LWA array at three frequencies within the operating bandwidth are reported in Fig. 11, for H- and E-planes. It can be observed from Fig. 11(a) that the θ_{3dB} beamwidth of radiation pattern decreases from $\pm 5^\circ$ to $\pm 2.9^\circ$ with the increase of frequency from 8 to 24 GHz. Similarly, θ_{3dB} beamwidth of radiation pattern in E-plane (given in Fig. 11(b)), varies $\pm 32.5^\circ$ to $\pm 20^\circ$ within the operating bandwidth. These results characterize the directive radiation of connected and perforated LWA array in one-plane and the desired fan-beam characteristic in the other plane which is necessary for 3-D body scanning systems. The interferences of multiple reflections within the lens result in oscillation of the directivity curves in absence of dielectric coatings [26]. The directivity variations with frequency in Fig. 12 show that there are no ripples in the directivity curves. This proves the effectiveness of the flaring part in the quasi-planar antenna, the three MLs or the perforations in connected arrays in avoiding reflections at the lens top interface. At higher frequencies up from 18 GHz, the directivity of the perforated array remains stable up on 18 GHz. In dense dielectric lens antenna applications although the MLs or other types of coatings prevent strong reflections, 3-dB beamwidth can still significantly vary with frequency. However, the directivity variation of perforated array highlights the frequency stability of the main beam between 18 GHz and 24 GHz frequencies. One can note that the single antenna has comparable gain with respect to the array, since it is terminated with a metal flaring which implements matching to free space and increases the gain. The flaring is not used in the array design, where a similar gain improvement is obtained with the array factor.

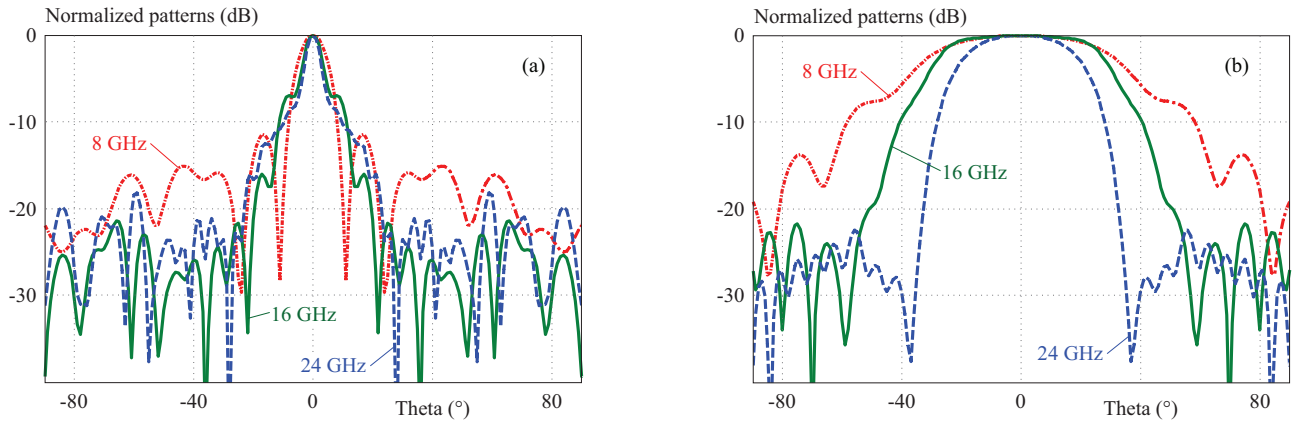

Fig. 11. Normalized radiation patterns in: (a) – H -plane, and (b) – E -plane at the frequencies 8, 16 and 24 GHz

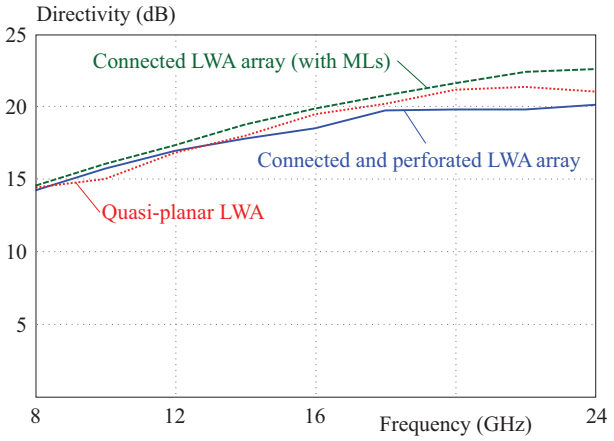

Fig. 12. Broadside directivity values with respect to frequency

5 Conclusion

We presented the design of a broadband dielectric lens antenna array, based on the lateral wave radiation phenomenon. The antenna consists of a number of PPW elements realizing two-dimensional focusing structures, stacked in an array configuration. The overall height of the stack is $0.54\,\lambda$ at the lowest frequency of operation, thus it is large enough to enable radiation in free space, without the need of additional metal flaring. Therefore, while each individual PPW element would be strongly mismatched at its open end, the assembly of more elements in a connected array environment allows achieving very broadband impedance matching, from 8 to 24 GHz. We showed that multiple dielectric MLs play a crucial role to reduce internal reflections. Nevertheless, this approach requires the use of different materials fabricated and assembled to the lens surface with the risk of creating air gaps between the lens and the coating due to the tolerance of the surface curvatures. Thus, proper perforations are employed to the top of lens material to approximate lower effective dielectric constant regions. The connected array accomplishes the frequency stability of radiation patterns at high frequencies of the operation band. Simulation results were shown to assess the effectiveness of the design improvements, aiming at decreasing the cost and complexity of the manufacturing process. The presented antenna array is a promising design to be used in three-dimensional body scanning systems.

Acknowledgment

This work was supported by Research Fund of the Yildiz Technical University. Project Number: FBA-2017-7-3070.

References

[1] D. Sheen, D. McMakin, and T. Hall, "Three-Dimensional Millimeter-Wave Imaging for Concealed Weapon Detection", *IEEE Transactions on Microwave Theory and Techniques*, vol. 49, no. 9, pp. 1581–1592, 2001, Available: 10.1109/22.942570.

[2] C. Rappaport and B. Gonzalez-Valdes, "The Blade Beam Reflector Antenna for Stacked Near Field Millimeter-Wave Imaging", *IEEE Int. Symp. Antennas Propag.*, Chicago, USA, 2012, pp. 1–4.

[3] C. Hua, N. Yang, X. Wu, and W. Wu, "Millimeter-Wave Fan-Beam Antenna Based on Step-Index Cylindrical Homogeneous Lens", *IEEE Antennas and Wireless Propag. Letters*, vol. 11, pp. 1512–1516, 2012.

[4] F. Yang, X. Wu, J. Zhou, and H. Shao, "Beam-Scanning Lens Antenna Based on Corrugated Parallel-Plate Waveguides", *IEEE Antennas and Wireless Propag. Letters*, vol. 17, no. 7, pp. 1296–1299, 2018.

[5] F. Tokan, N. T. Tokan, A. Neto, and D. Cavallo, "The Lateral Wave Antenna", *IEEE Trans. Antennas Propag.*, vol. 62, no. 6, pp. 2909–2916, 2014.

[6] M. J. M. Van Der Vorst, P. J. I. De Maagt, A. Neto, A. L. Reynolds, and R. M. Heeres, "Effect of Internal Reflections on the Radiation Properties and Input Impedance of Integrated Lens Antennas-Comparison between Theory and Measurements", *IEEE Trans. Microw. Theory and Tech.*, vol. 49, no. 6, pp. 1118–1125, 2001.

[7] M. J. M. Van Der Vorst, P. J. I. De Maagt, and M. A. J Herben, "Effect of Internal Reflections on the Radiation Properties and Input Admittance of Integrated Lens Antennas", *IEEE Trans. Microw. Theory and Tech.*, vol. 47, no. 9, pp. 1696–1704, 1999.

[8] N. T. Nguyen, R. Sauleau, and C. J. Martinez-Perez, "Very Broadband Extended Hemispherical Lenses: Role of Matching Layers for Bandwidth Enlargement", *IEEE Trans. Antennas Propag.*, vol. 57, no. 7, pp. 1907–1913, 2009.

[9] , Microwave Studio. [Online]. Available: http://www.cst.com/.

[10] A. Wang, D. Fang, B. Zhang, and W. Che, "Dielectric Loaded Substrate Integrated Waveguide (SIW) H-Plane Horn Antennas", *IEEE Trans. Antennas Propag.*, vol. 58, no. 3, pp. 640–647, 2010.

[11] A. R. Mallahzadeh and S. Esfandiarpour, "Wideband H-Plane Horn Antenna Based on Ridge Substrate Integrated Waveguide (RSIW)", *IEEE Antennas and Wireless Propag. Letters*, vol. 11, pp. 85–88, 2012.

[12] P. S. Kildal, "Bandwidth of a Square Hard Horn", *IEE Proc. H-Microwaves, Antennas and Propagation*, vol. 135, no. 4, pp. 275–278, August 1988.

[13] K. Chung, S. Pyun, and Ja. Choi, "Design of an Ultrawide-Band TEM Horn Antenna with a Microstrip-Type Balun", *IEEE Trans. Antennas Propag.*, vol. 53, no. 10, pp. 3410–3413, 2005.

[14] N. T. Tokan, A. Neto, F. Tokan, and D. Cavallo, "Comparative Study on Pulse Distortion and Phase Aberration of Directive Ultra-Wideband Antennas", *IET Microw. Antennas Propag.*, vol. 7, no. 12, pp. 1021–1026, 2013.

[15] R. C. Hansen, "Linear Connected Arrays", *IEEE Antennas and Wireless Propag. Letters*, vol. 3, pp. 154–156, 2004.

[16] Y. Yao, M. Liu, W. Chen, and Z. Feng, "Analysis and Design of Wideband Widescan Planar Tapered Slot Antenna Array", *IET Microw. Antennas Propag.*, vol. 4, no. 10, pp. 1632–1638, 2010.

[17] A. Neto, D. Cavallo, G. Gerini, and G. Toso, "Scanning Performances of Wideband Connected Arrays the Presence of a Backing Reflector", *IEEE Trans. Antennas Propag.*, vol. 57, no. 10, pp. 3092–3102, 2009.

[18] D. M. Pozar, "A Relation between the Active Input Impedance and the Active Element Pattern of a Phased Array", *IEEE Trans. Antennas Propag.*, vol. 51, no. 9, pp. 2486–2489, 2003.

[19] N. T. Sönmez and N. T. Tokan, "Effects of Antireflective Coatings on Scanning Performance of Millimetre-Wave Lenses", *IET Microw. Antennas Propag.*, vol. 10, no. 14, pp. 1485–1491, 2016.

[20] F. Tokan, "Optimization-Based Matching Layer Design for Broadband Dielectric Lens Antennas", *Applied Comp. Electromagn. Soc. Journal*, vol. 29, no. 6, pp. 499–507, 2014.

[21] N. T. Nguyen, N. Delhote, M. Ettore, D. Baillargeat, and L. LeCoq *et al*, "Design and Characterization of 60-GHz Integrated Lens Antennas Fabricated through Ceramic Stereolithography", *IEEE Trans. Antennas Propag.*, vol. 58, no. 8, pp. 2757–2762, 2010.

[22] S. Biber, J. Richter, S. Martius, and L. -P. Schmidt, "Design of Artificial Dielectrics for Anti-Reflection-Coatings", *Proc. 33rd Eur. Microw. Conf.*, Munich, Germany, September 2003, vol. 3, pp. 1115-1118.

[23] A. Petosa and A. Ittipiboon, "Design and Performance of a Perforated Dielectric Fresnel Lens", *IEE Proceedings-Microw. Antennas and Propag.*, vol. 150, no. 5, pp. 309–314, 2003.

[24] J. S. Colburn and Y. Rahmat-Samii, "Patch Antennas on Externally Perforated High Dielectric Constant Substrates", *IEEE Trans. Antennas Propag.*, vol. 47, no. 12, pp. 1785–1794, 1999.

[25] M. Mrnka and Z. Raida, "An Effective Permittivity Tensor of Cylindrically Perforated Dielectrics", *IEEE Antennas and Wireless Propag. Letters*, vol. 17, no. 1, pp. 66–69, 2018.

[26] A. Darvazehban, O. Manoochehri, M. Salari, A. Emadeddin, and D. Erricolo, "A Parallel Plate Ultrawideband Multi-Beam Microwave Lens Antenna", *IEEE Trans. Antennas Propag.*, vol. 66, no. 9, pp. 4878–4883, 2018.

Received 18 August 2020

Fikret Tokan received his PhD degree from Yildiz Technical University, Istanbul, in Communication Engineering in 2010. From October 2011 to October 2012, he was Postdoctoral Researcher in the EEMCS Department of Delft University of Technology. From October 2012 to May 2013, he was a Postdoctoral Fellow at the Institute of Electronics and Telecomm. (IETR), University of Rennes 1, France. Since September 2002, he has been working in the Electromagnetic Fields and Microwave Technique Section of the Electronics and Communications Engineering Department of Yildiz Technical University. He has been currently working as an Assoc Prof at that department. His current research interests are UWB antenna design, dielectric lens antennas, reflector systems, electromagnetic waves, propagation, antenna arrays, scattering and numerical methods.

Daniele Cavallo (S'09M'11SM'19) received the MSc degree (summa cum laude) in telecommunication engineering from the University of Sannio, Benevento, Italy, in 2007, and the PhD degree (cum laude) in electromagnetics from Eindhoven University of Technology (TU/e), Eindhoven, The Netherlands, in 2011. From 2007 to 2011, he was with the Antenna Group, Netherlands Organization for Applied Scientific Research (TNO), The Hague, The Netherlands. From 2012 to 2015, he was a Post-Doctoral Researcher with the Microelectronics Department, Delft University of Technology (TU Delft), Delft, The Netherlands. In 2015, he joined the Chalmers University of Technology, Gothenburg, Sweden, as a Visiting Researcher. He is currently an Assistant Professor with the Terahertz Sensing Group, TU Delft. His current research interests include analytical and numerical methods for antenna characterization, the design of antenna arrays, and on-chip antennas.

Andrea Neto received the Laurea degree (summa cum laude) in electronic engineering from the University of Florence, in 1994 and the PhD degree in electromagnetics from the University of Siena, Italy, in 2000. From 2000 to 2001, he was a Post-Doctoral Researcher with the California Institute of Technology, Pasadena, CA, USA, where he worked with the Sub-Millimeter Wave Advanced Technology Group. From 2002 to January 2010, he was a Senior Antenna Scientist with TNO Defence, Security, and Safety, The Hague, The Netherlands. In February 2010, he became a Full Professor of applied electromagnetism with the Electrical Engineering, Mathematics and Computer Science (EEMCS) Department, Technical University of Delft, The Netherlands, where he formed and leads the THz Sensing Group. His research interests include the analysis and design of antennas with an emphasis on arrays, dielectric lens antennas, wideband antennas, EBG structures, and THz antennas.